Laser-based trajectory tracking $\mathcal{H}_2$ control of autonomous rotorcraft

B. J. Guerreiro * **C. Silvestre** * **R. Cunha** *

* *Instituto Superior Técnico, Institute for Systems and Robotics Av. Rovisco Pais, 1, 1049-001 Lisboa, Portugal*
{bguerreiro,cjs,rita}@isr.ist.utl.pt

Abstract: This paper proposes a laser-based trajectory tracking control methodology for rotorcraft operation in environments where absolute position measurements are unavailable or unreliable. Laser-based nonlinear kinematics are formulated in three-dimensions space, and a trajectory-dependent error space is defined to express the dynamic model of the vehicle and the laser-based kinematics. A linear parameter varying (LPV) representation with piecewise affine dependence on the parameters is introduced to model the error dynamics over a set of predefined operating regions. The synthesis problem is stated as a continuous-time $\mathcal{H}_2$ control problem, solved using linear matrix inequalities (LMIs) and implemented within the scope of gain-scheduling control theory. The effectiveness of the proposed controller is assessed in simulation using the full nonlinear model of a small-scale helicopter.

Keywords: Laser-based control, autonomous vehicles, helicopter control, disturbance rejection.

1. INTRODUCTION

This paper proposes a trajectory tracking control methodology for autonomous rotorcraft, based on laser scanning sensors, for mission environments where absolute position measurements are unavailable or unreliable. The envisaged application of the technique herein proposed is the automatic inspection of bridge piers, for which autonomous helicopters are one of the most appropriated tools.

Bridge structural components, such as the deck and piers, are affected in their strength and durability by age, aggressive environment and steadily increasing traffic, especially in places where design, construction or maintenance errors are committed (Parke and Hewson, 2008). It is essential for large infrastructures like bridges to be subject to regular maintenance inspections and procedures in order to enable early detection of any defect which may cause unacceptable safety or serviceability risks or serious maintenance requirements. Otherwise, the consequences widen up from complex remedial or maintenance actions to loss of structural, environmental or public safety integrity. The maintenance cost and risk reduction stemming from the replacement of the standard procedures and the improved detection of structural defects, confirm the future use of automatic structure inspection tools, for which autonomous helicopters are natural platforms that can carry multiple sensors, like infrared cameras, sonar or radar sensor systems.

[1] This work was partially supported by Fundação para a Ciência e a Tecnologia (ISR/IST pluriannual funding) through the POS_Conhecimento Program that includes FEDER funds and by the PTDC/EEA-ACR/72853/2006 HELICIM project. The work of B. J. Guerreiro was supported by PhD Student Grant SFRH/BD/21781/2005 from the Portuguese FCT POCTI programme.

In the present scenario, the helicopter is expected to describe helices around a bridge pier, searching for structural defects, and also hover at exact positions relative to the pier to monitor particular characteristics, assess maintenance or repair requirements, as illustrated in Figure 1. In this context, the development of laser-based trajectory tracking control systems constitutes both a challenge and a fundamental requirement for accomplishing high performance autonomous flight without absolute positioning measurements.

The use of ranging sensors to obtain vehicle localization in GPS-denied [2] environments is by now an ubiquitous and mandatory technology in mobile robots (Leonard and Durrant-Whyte, 1991; Thrun et al., 2001). However, in the field of unmanned aerial vehicles (UAVs) this problem has only been addressed in recent years (He et al., 2008),

[2] GPS – Global Positioning System

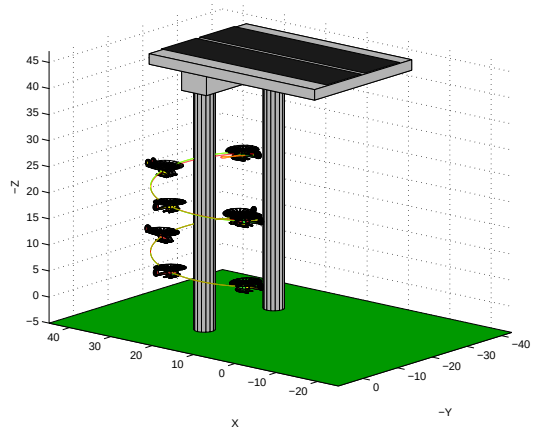

Fig. 1. Inspection scenario and 3-D trajectory

and mainly assuming full knowledge of the geometry of the world where the UAV has to localize itself. The approach proposed in this paper does not aim at providing a localization algorithm, but rather to find a simple and reliable control methodology that enables automatic inspection of large infrastructures, under mild geometric assumptions.

The presented solution relies on the formulation of nonlinear laser kinematics in order to obtain the position of the vehicle relative to the structure to be inspected. It is considered that both a laser scanner and a range only scanner are used in order to get measurements on the horizontal plane and vertical axis, respectively. A trajectory-dependent error space is defined to express the dynamic model of the vehicle. The error vector, which the trajectory-tracking controller should drive to zero, comprises linear and angular velocities, and orientation errors relatively to the reference trajectory, as well as position errors based on the laser kinematics.

Linear Matrix Inequalities (LMIs) used together with Linear Parameter Varying models (LPVs) constitute a powerful tool for tackling difficult nonlinear problems. Several examples in the literature attest for its level of success (Guerreiro et al., 2007; Cunha et al., 2006). This paper adopts an LPV representation with piecewise affine dependence on the parameters to accurately model the error dynamics over a predefined set of operating regions. By imposing an affine parameter dependence, a continuous-time $\mathcal{H}_2$ state feedback controller can be derived in order to guarantee $\mathcal{H}_2$ performance over a convex set of parameters using a finite number of LMIs. Based on this result, a controller is synthesized for each of the operating regions and the resulting controller is implemented within the framework of gain-scheduling control theory using the D-methodology (Kaminer et al., 1995).

This paper is organized as follows. Section 2 presents a brief summary of the helicopter dynamic model, while Section 3 proposes the laser kinematics. In Section 4 the trajectory-dependent error space is introduced and Section 5 deals with the control synthesis. Implementation issues and the simulation results are presented in Section 6 and a summary of the main ideas and contributions of this paper are given in Section 7.

2. HELICOPTER DYNAMIC MODEL

This section summarizes the helicopter dynamic model. A comprehensive coverage of helicopter flight dynamics can be found in (Padfield, 1996) and (Cunha, 2002; Cunha et al., 2005), where this model is described in more detail.

Consider the helicopter modeled as a rigid body driven by forces and moments applied to the helicopter's center of mass that include the contribution of the main rotor, tail rotor, fuselage, horizontal tail plane, vertical tail fin, and gravity. Consider the following frames:

- $\{I\}$ – Inertial frame: the horizontal plane is defined by the x and y axis and the z-axis is vertical and points downwards.
- $\{B\}$ – Body-fixed frame: Origin at the center of mass of the vehicle, x-axis pointing forward and the z-axis point downwards. The transformation that maps points in frame $\{B\}$ to points in frame $\{I\}$ is defined by ${}^I\mathbf{p}_i = {}^I_B R\, {}^B p_i + {}^I p_B$.

The notation used throughout this paper considers that the subscript and superscript in a rotation matrix indicate the original and transformed frames, respectively, as in (Craig, 1986). Let $\left({}^I\mathbf{p}_B, {}^I_B R\right) \in SE(3) \triangleq \mathbb{R}^3 \times SO(3)$ denote the configuration of $\{B\}$ relative to $\{I\}$ where ${}^I_B R$ can be parameterized by the Z-Y-X Euler angles $\boldsymbol{\lambda} = [\,\phi\ \theta\ \psi\,]^T$, with $\theta \in]-\frac{\pi}{2}, \frac{\pi}{2}[$, $\phi, \psi \in \mathbb{R}$, resulting in ${}^I_B R = R_z(\psi)\, R_y(\theta)\, R_x(\phi)$, where the rotation matrix $R_a(b)$ stands for the basic rotation of an angle b about the a-axis. In addition, let the linear and angular velocities be given by $\mathbf{v} = [u\ v\ w]'$ and $\boldsymbol{\omega} = [p\ q\ r]'$, respectively, and consider the simplified notation for the position vector, $\mathbf{p} = {}^I\mathbf{p}_B$, and for the rotation matrix, $\mathcal{R} = {}^I_B R$.

Hence, the helicopter state equations, combining kinematics and dynamics, can be written as

$$\dot{\mathbf{v}} = -\boldsymbol{\omega} \times \mathbf{v} + \tfrac{1}{m}\left[\mathbf{f}\left(\mathbf{v}, \boldsymbol{\omega}, \mathbf{u}, \mathbf{v}_w\right) + \mathbf{f}_g\left(\phi, \theta\right)\right] \quad (1)$$

$$\dot{\boldsymbol{\omega}} = I^{-1}\left[-\boldsymbol{\omega} \times I\,\boldsymbol{\omega} + \mathbf{n}\left(\mathbf{v}, \boldsymbol{\omega}, \mathbf{u}, \mathbf{v}_w\right)\right] \quad (2)$$

$$\dot{\mathbf{p}} = \mathcal{R}\left(\boldsymbol{\lambda}\right)\mathbf{v} \quad (3)$$

$$\dot{\boldsymbol{\lambda}} = \mathcal{Q}\left(\phi, \theta\right)\boldsymbol{\omega} \quad (4)$$

where m is the vehicle mass, I is the tensor of inertia about the frame $\{B\}$, $\mathbf{u}$ is the input vector, $\mathbf{v}_w$ is the wind velocity vector expressed in $\{B\}$, $\mathbf{f}_g$ represents the gravitational force vector and $\mathbf{f}$ and $\mathbf{n}$ denote the remaining external forces and moments applied to the vehicle. Matrix $\mathcal{Q}$ relates the vehicle angular velocity with the time derivative of the Euler angles. The input vector $\mathbf{u} = [\theta_{c_0}\ \theta_{c_{1c}}\ \theta_{c_{1s}}\ \theta_{c_{0t}}]'$ comprises the main rotor collective, longitudinal cyclic and lateral cyclic blade pitch angle commands, and the tail rotor collective blade pitch angle command, respectively. The force and moment vectors, $\mathbf{f}$ and $\mathbf{n}$, can be further decomposed as $\mathbf{f} = \mathbf{f}_{mr} + \mathbf{f}_{tr} + \mathbf{f}_{fus} + \mathbf{f}_{tp} + \mathbf{f}_{fn}$ and $\mathbf{n} = \mathbf{n}_{mr} + \mathbf{n}_{tr} + \mathbf{n}_{fus} + \mathbf{n}_{tp} + \mathbf{n}_{fn}$, where the subscripts mr, tr, fus, tp and fn stand for main rotor, tail rotor, fuselage, horizontal tail plane and vertical tail fin, respectively. Note that depending on the complexity of model considered for the blade flap and pitch motions, additional state variables may be required. Also, the disturbance input $\mathbf{v}_w$ can be modeled as a random process with a predefined power spectral density (PSD) such as the von Karman turbulence model, or using the statistical discrete gust approach (SDG), essentially employed to cater for more structured disturbances. For in depth coverage of this topic the reader is referred to (Padfield, 1996), and references therein.

Note that the position kinematics in (3) is only showed for completeness, since this equation will be replaced by the laser-based kinematics presented in the next section.

3. LASER KINEMATICS

The main focus of the this work is the control of rotorcraft along suitable trajectories in order to achieve effective inspection of bridge piers. For this purpose, the admissible trajectories of the helicopter are reduced to helices and hover at a given distance from the pier.

In order to thoroughly define the laser kinematics the following additional frames are introduced:

$\{L\}$ – Laser frame: Origin at the laser beam firing point, x-axis indicating the zero scanning angle and the scanning angle is defined as a rotation about the z-axis. The transformation that maps points in frame $\{B\}$ to points in frame $\{L\}$ is defined by ${}^{L}\mathbf{p}_i = {}^{L}_{B}R\,{}^{B}p_i + {}^{L}p_B$.

$\{LP\}$ – Laser projected frame: origin coincident with frame $\{L\}$ with x and y-axis projected into the horizontal plane. The transformation that maps points in frame $\{L\}$ to points in frame $\{LP\}$ is defined by ${}^{LP}\mathbf{p}_i = {}^{LP}_{L}R\,{}^{L}p_i$, where ${}^{LP}_{L}R = R_y(\theta)\,R_x(\phi)$.

Consider also that at each sampling instant, the laser provides a set of n_L laser data points (ρ_i, α_i), for $i = 1, \ldots, n_L$, where ρ_i stands for the range distance measurement and α_i is the respective angle.

The main assumptions on which the development of the laser space kinematics is based are presented below. The first assumption concerns the measurements that are available for the kinematics computations.

Assumption 1. There is no access to absolute position measurements. Good estimates of velocities and attitude are provided.

Assumption 1 implies that the state variables $\mathbf{v}_B$, $\boldsymbol{\omega}_B$, and $\boldsymbol{\lambda}_B$ can be used. The second assumption aims only at the simplification of the expressions presented in this section and does not imply any loss of generality of the control method.

Assumption 2. The frames $\{B\}$ and $\{L\}$ are coincident, meaning that ${}^{L}_{B}R = I_{3\times3}$ and ${}^{L}p_B = \mathbf{0}_{3\times1}$.

The next assumption concerns the shape of the piers and reflects the main application of this control methodology, which is the automatic inspection of concrete bridges piers.

Assumption 3. The piers of the bridge are similar to a vertical cylindrical volume.

Concrete bridge piers usually have cylindrical volume or at least a rectangular section. This last shape can also be tackled by the proposed methodology as will be discussed later. One further assumption is made about the ground surrounding the inspection area, as stated below.

Assumption 4. The ground surrounding the inspection area is assumed to be an horizontal plane.

3.1 Pier geometry and center position computation

The main focus after acquiring the laser measurements is to detect invariant points from which we can infer the relative position of the helicopter. This task is specially daunting in frames $\{L\}$ or $\{B\}$. For this reason, and assuming only knowledge of the roll and pitch angles of the vehicle, ϕ and θ, the original measurements of the LADAR, (ρ_i, α_i), are transformed to their projection in frame $\{LP\}$, denoted as $({}^{LP}\rho_i, {}^{LP}\alpha_i)$. The relation between range and angular information in $\{L\}$ and $\{LP\}$ can be expressed as

$$
\begin{aligned}
{}^{LP}\rho_i^2 = \rho_i^2\,[&(\cos(\alpha_i)\,\cos(\theta) + \sin(\alpha_i)\,\sin(\phi)\,\sin(\theta))^2 \\
&+(\sin(\alpha_i)\,\cos(\phi))^2]\,,
\end{aligned}
$$

$$
\tan({}^{LP}\alpha_i) = \frac{\sin(\alpha_i)\,\cos(\phi)}{\cos(\alpha_i)\,\cos(\theta) + \sin(\alpha_i)\,\sin(\phi)\,\sin(\theta)}\,.
$$

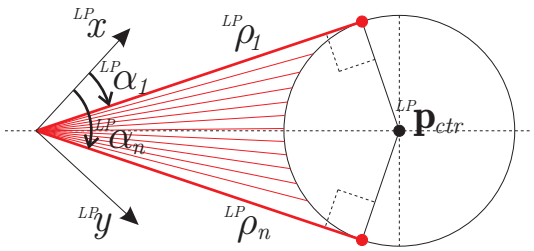

Fig. 2. Laser measurements

It is a fact that the intersection of any vertical cylindrical pier with the plane defined by the x and y-axis of frame $\{LP\}$ yields a circle. In this way, the laser measurements $({}^{LP}\rho_i, {}^{LP}\alpha_i)$ that represent the pier also represent an arc of a circle. Using basic notions of geometry, it can be seen that, given any point outside the circle and in the same plane, there are only two lines that pass through this point and are tangent to the circle, as shown in Figure 2. These lines are approximated by the first and last laser measurement that intersects the pier, provided that the angular resolution of the laser is sufficiently high.

Therefore, the center of the pier is estimated using the first and last laser measurements transformed into the $\{LP\}$ frame, respectively $({}^{LP}\rho_1, {}^{LP}\alpha_1)$ and $({}^{LP}\rho_n, {}^{LP}\alpha_n)$, where n is the number of laser measurements that intersect the pier. The expressions for the equivalent range and angle of the center of the pier are given by

$$
{}^{LP}\rho_{ctr} = \frac{{}^{LP}\rho_1 + {}^{LP}\rho_n}{2\,\cos(\frac{{}^{LP}\alpha_n - {}^{LP}\alpha_1}{2})}\,,\quad {}^{LP}\alpha_{ctr} = \frac{{}^{LP}\alpha_1 + {}^{LP}\alpha_n}{2}\,.
$$

The fact that only the first and last measurements of the laser are used to estimate the center of the pier indicates that if its shape is not exactly a cylinder, the algorithm will still be valid. Naturally, the width of the pier measured by the laser will not have a direct relation with the its center, contrary to what is obtained with a cylindrical pier.

3.2 Ground measurement

In order to have a complete 3-D position measurement an additional altitude sensor is needed. In the approach presented in this work it is assumed that an additional range only laser sensor is placed in the vehicle in order to acquire the distance to the ground along the z-axis of the laser frame $\{L\}$. For simplicity, and once again without loss of generality, it is assumed that both laser systems (the laser scanner on the xoy plane and the range only laser in the z-axis) share the same reference frame, $\{L\}$. Considering Assumption 4 and the fact that the pitch and roll angles are known, the distance-to-ground measurement in frame $\{L\}$, denoted as ${}^{L}z_{hg}$, can be projected into the z-axis of frame $\{LP\}$ using the expression

$$
{}^{LP}z_{hg} = {}^{L}z_{hg}\,\cos\phi\,\cos\theta\,.
$$

Note that this somehow restrictive assumption could be easily overcome with the usage of an additional laser scanner placed in the yoz plane of frame $\{LP\}$, replacing the range only sensor in the z-axis.

3.3 Laser kinematics

The equations of motion for the laser kinematics are naturally divided into the horizontal plane and the vertical axis

kinematics, corresponding to the two different laser sensors previously referred. Nonetheless, they can be considered as a unique sensor that provides the position of the center of the pier at ground level, which can be expressed as

$$ {}^{LP}\mathbf{p}_{ctr} = R_z({}^{LP}\alpha_{ctr}) \begin{bmatrix} {}^{LP}\rho_{ctr} \\ 0 \\ {}^{LP}z_{hg} \end{bmatrix} , $$

with time derivative given by

$$ {}^{LP}\dot{\mathbf{p}}_{ctr} = R_z({}^{LP}\alpha_{ctr}) \begin{bmatrix} {}^{LP}\dot{\rho}_{ctr} \\ {}^{LP}\rho_{ctr}\,{}^{LP}\dot{\alpha}\_ctr \\ {}^{LP}\dot{z}_{hg} \end{bmatrix} . \quad (5) $$

Moreover, the same point can be expressed as

$$ {}^{LP}\mathbf{p}_{ctr} = {}^{LP}_{I}R({}^{I}\mathbf{p}_{ctr} - {}^{I}\mathbf{p}_{B}) , $$

and its time derivative, as a function of the vehicle velocities, can be written as

$$ {}^{LP}\dot{\mathbf{p}}_{ctr} = -S(\Pi_z\,\boldsymbol{\omega})\,{}^{LP}\mathbf{p}_{ctr} - {}^{LP}_{B}R\,\mathbf{v} , \quad (6) $$

where the skew-symmetric matrix $S(.)$ denotes the cross product matrix operator, $S(\mathbf{a})\,\mathbf{b} = \mathbf{a} \times \mathbf{b}$, and $\Pi_z = \text{diag}([0\ 0\ 1])$ is the projection matrix onto the z-axis[3].

Combining Equations (5) and (6) in order to obtain the differential equations that define the laser based kinematics results, after some algebraic manipulation, in

$$ \begin{bmatrix} {}^{LP}\dot{\rho}_{ctr} \\ {}^{LP}\dot{\alpha}_{ctr} \\ {}^{LP}\dot{z}_{hg} \end{bmatrix} = \mathbf{r}(r) - I_y({}^{LP}\rho_{ctr})\,R'_z({}^{LP}\alpha_{ctr})\,{}^{LP}_{B}R\,\mathbf{v} , $$

where $\mathbf{r}(r) = [0\ -r\ 0]'$, ${}^{LP}_{B}R = R_y(\theta)\,R_x(\phi)$ and $I_y(a) = \text{diag}([1\ 1/a\ 1])$. For the sake of simplicity, the superscript ^{LP} and the subscript ${}_{ctr}$ are dropped for the remainder of this article. Letting the generalized laser-based position vector be defined as $\boldsymbol{\eta} = [\rho\ \alpha\ z_{hg}]'$, the laser-based kinematics equation can be rewritten as

$$ \dot{\boldsymbol{\eta}} = \mathbf{r}(r) - I_y(\rho)\,R'_z(\alpha)\,R_y(\theta)\,R_x(\phi)\,\mathbf{v} . \quad (7) $$

4. GENERALIZED ERROR DYNAMICS

This section introduces the concept of trimming trajectories for the helicopter model, presents a generalized error space to describe the helicopter's motion about trimming trajectories, and computes explicitly the helicopter dynamics in the new error space.

Consider the helicopter equations of motion presented in (1), (2), (4), and (7), and let $\mathbf{v}_c$, $\boldsymbol{\omega}_c$, $\boldsymbol{\eta}_c$, $\boldsymbol{\lambda}_c$, and $\mathbf{u}_c$ denote the trimming values of the state and input vectors. At trimming, these vectors satisfy $\dot{\mathbf{v}}_c = \mathbf{0}$, and $\dot{\boldsymbol{\omega}}_c = \mathbf{0}$ implying that $\dot{\mathbf{u}}_c = \mathbf{0}$, $\dot{\phi}_c = 0$, and $\dot{\theta}_c = 0$. Given the dependence of the gravitational terms on the roll and pitch angles, only the yaw angle can change without violating the equilibrium condition. However, ψ_c satisfies $\begin{bmatrix} 0\ 0\ \dot{\psi}_c \end{bmatrix}' = Q\,(\phi_c, \theta_c)\,\boldsymbol{\omega}_c$ and thus the yaw rate, $\dot{\psi}_c$, is constant. For the envisaged application, the trimming trajectories of interest are only z aligned helices and hover, characterized by constant values of ρ_c and α_c. These trajectories can be described by the parametrization $\boldsymbol{\xi}_L = \begin{bmatrix} \rho_c\,\alpha_c\,\dot{\psi}_c\,v_{z_c} \end{bmatrix}'$, where ρ_c is desired value of the distance to the pier, α_c is the azimuth of the pier in $\{LP\}$ and v_{z_c} is the z component of the velocity vector described in $\{LP\}$. This set of parameters can be mapped onto the more general parametrization, defined by

$$ \boldsymbol{\xi} = \begin{bmatrix} V_c\,\gamma_c\,\dot{\psi}_c\,\psi_{ct} \end{bmatrix}' , \quad (8) $$

which fully parameterizes the set of achievable helicopter trimming trajectories (Cunha, 2002), where $V_c = \|\mathbf{v}_c\|$ is the linear body speed, γ_c the flight-path angle, and ψ_{ct} the yaw angle of the helicopter relative to the tangent to the path.

The generalized error vector defined between the vehicle state and the commanded trajectory can be defined using the nonlinear transformation

$$ \mathbf{x}_e = \begin{bmatrix} \mathbf{v}_e \\ \boldsymbol{\omega}_e \\ \boldsymbol{\eta}_e \\ \boldsymbol{\lambda}_e \end{bmatrix} = \begin{bmatrix} \mathbf{v} - \mathbf{v}_c \\ \boldsymbol{\omega} - \boldsymbol{\omega}_c \\ \boldsymbol{\eta} - \boldsymbol{\eta}_c \\ \mathcal{Q}^{-1}\,(\boldsymbol{\lambda} - \boldsymbol{\lambda}_c) \end{bmatrix} . \quad (9) $$

In addition, let $\mathbf{u}_e = \mathbf{u} - \mathbf{u}_c$ and $\mathbf{v}_{w_e} = \mathbf{v}_w$, assuming that there is no disturbance at trimming, $\mathbf{v}_{w_c} = 0$. It can be shown that in the new error coordinate system the linearization of the rigid body dynamics given by (1), (2), (4), and (7) along any arbitrary trimming trajectory is time invariant, see (Silvestre, 2000) for further details. The nonlinear error dynamics can then be expressed as

$$ \begin{cases} \dot{\mathbf{v}}_e = \dot{\mathbf{v}} \\ \dot{\boldsymbol{\omega}}_e = \dot{\boldsymbol{\omega}} \\ \dot{\boldsymbol{\eta}}_e = \dot{\boldsymbol{\eta}} \\ \dot{\boldsymbol{\lambda}}_e = \boldsymbol{\omega} - \mathcal{Q}^{-1}\,\mathcal{Q}_c\,\boldsymbol{\omega}_c - \dfrac{d}{dt}\mathcal{Q}^{-1}\,\mathcal{Q}\,\boldsymbol{\lambda}_e, \end{cases} \quad (10) $$

noting that $\dot{\mathbf{v}}_c = 0$ and $\dot{\boldsymbol{\omega}}_c = 0$ for any trimming trajectory, and defining $\mathcal{R}_e^{-1} = \mathcal{R}^{-1}\,\mathcal{R}_c$, $\mathcal{Q}_e = \mathcal{Q}\,(\boldsymbol{\lambda}_e)$ and $S(\boldsymbol{\omega})$ as the skew symmetric matrix given by $S(\boldsymbol{\omega}) = [\boldsymbol{\omega}\times]$. The linearization of (10) about the zero, or equivalently, the linearization of (1), (2), (4), and (7) about the trimming trajectory can be expressed in the generalized error space as

$$ \begin{array}{rcl} \delta\dot{\mathbf{v}}_e &=& A_v^v\,\delta\mathbf{v}_e + A_v^\omega\,\delta\boldsymbol{\omega}_e + A_v^\lambda\,\delta\boldsymbol{\lambda}_e + B_v\,\delta\mathbf{u}_e + B_{w_v}\,\delta\mathbf{v}_w \\ \delta\dot{\boldsymbol{\omega}}_e &=& A_\omega^v\,\delta\mathbf{v}_e + A_\omega^\omega\,\delta\boldsymbol{\omega}_e + A_\omega^\lambda\,\delta\boldsymbol{\lambda}_e + B_\omega\,\delta\mathbf{u}_e + B_{w_\omega}\,\delta\mathbf{v}_w \\ \delta\dot{\boldsymbol{\eta}}_e &=& A_\eta^v\,\delta\mathbf{v}_e + A_\eta^\omega\,\delta\boldsymbol{\omega}_e + A_\eta^\eta\,\delta\boldsymbol{\eta}_e + A_\eta^\lambda\,\delta\boldsymbol{\lambda}_e \\ \delta\dot{\boldsymbol{\lambda}}_e &=& \delta\boldsymbol{\omega}_e - S(\boldsymbol{\omega}_c)\,\delta\boldsymbol{\lambda}_e \end{array} \quad (11) $$

where $A_x^y = \left.\frac{\partial}{\partial\mathbf{y}}\mathbf{f}_x(.)\right|_c$ are constant matrices for each trimming trajectory, and $\mathbf{f}_x(.)$ represents the functions defined by Equations (1), (2), and (7). Rewriting (11) in a compact form gives

$$ \begin{array}{rcl} \delta\dot{\mathbf{x}}_e &=& A_e(\boldsymbol{\xi})\,\delta\mathbf{x}_e + B_{w_e}(\boldsymbol{\xi})\,\delta\mathbf{v}_w + B(\boldsymbol{\xi})\,\delta\mathbf{u}_e \\ \mathbf{z}_e &=& C_e(\boldsymbol{\xi})\,\delta\mathbf{x}_e + D_e(\boldsymbol{\xi})\,\delta\mathbf{v}_w + E(\boldsymbol{\xi})\,\delta\mathbf{u}_e. \end{array} $$

From this result it follows that there is a linear time invariant plant (11), associated to each trimming trajectory, for which a linear controller can be designed.

5. CONTROLLER SYNTHESIS

In this section an LMI approach is used to tackle the continuous-time state feedback $\mathcal{H}_2$ synthesis problem for polytopic LPV systems. Consider a LPV system

$$ \begin{array}{rcl} \dot{\mathbf{x}} &=& A(\boldsymbol{\xi})\mathbf{x} + B_w(\boldsymbol{\xi})\mathbf{w} + B(\boldsymbol{\xi})\mathbf{u} \\ \mathbf{z} &=& C(\boldsymbol{\xi})\mathbf{x} + D(\boldsymbol{\xi})\mathbf{w} + E(\boldsymbol{\xi})\mathbf{u} \end{array} \quad (12) $$

where $\mathbf{x}$ is the state, $\mathbf{u}$ is the control input, $\mathbf{z}$ denotes the error signal to be controlled, and $\mathbf{w}$ denotes the exogenous

[3] The operator diag(.) transforms a vector into a zero square matrix of appropriate dimensions with the diagonal elements equal to the elements of the vector.

input signal. The system is parameterized by $\boldsymbol{\xi}$, which is a possibly time-varying parameter vector and belongs to the convex set $\Xi = \text{co}(\Xi_0)$ where co(.) denotes the convex hull, Ξ_0 is the set of n_v vertices defined by $\Xi_0 = \{\boldsymbol{\xi} \in \mathbb{R}^{n_p} | \xi_i \in \{\underline{\xi}_i, \overline{\xi}_i\}, i = 1, \ldots, n_p\}$, where $\underline{\xi}_i \leq \overline{\xi}_i$, and the parameter set is defined by $\Xi = \{\boldsymbol{\xi} \in \mathbb{R}^{n_p} | \xi_i \in [\underline{\xi}_i, \overline{\xi}_i], i = 1, \ldots, n_p\}$.

Since the synthesis problem involves testing an infinite number of LMI's, several different structures for the LPV system have been proposed which reduce the problem to that of solving a finite number of LMI's. This paper adopts a polytopic description, which can be used to model a wide spectrum of systems and, as shown in the next section, is an adequate choice for the system at hand.

Definition 5. (Polytopic LPV system). The system (12) is said to be a polytopic LPV system if, for all $\boldsymbol{\xi} \in \Xi$, the system matrix $S(\boldsymbol{\xi}) = \begin{bmatrix} A(\boldsymbol{\xi}) & B_w(\boldsymbol{\xi}) & B(\boldsymbol{\xi}) \\ C(\boldsymbol{\xi}) & D(\boldsymbol{\xi}) & E(\boldsymbol{\xi}) \end{bmatrix}$ verifies $S(\boldsymbol{\xi}) \in \text{co}\,(S_1, \ldots, S_r)$, where co(.) denotes the convex hull operator and $S_i = \begin{bmatrix} A_i & B_{w_i} & B_i \\ C_i & D_i & E_i \end{bmatrix}$, for all $i = \{1, \ldots, r\}$.

The objective is to find a solution to the continuous-time state feedback $\mathcal{H}_2$ synthesis problem. Consider the static state feedback law given by $\mathbf{u} = K\mathbf{x}$ and let T_{zw} denote the closed loop operator from $\mathbf{w}$ to $\mathbf{z}$. Then, the $\mathcal{H}_2$ synthesis problem can be described as that of finding a control matrix K that stabilizes the closed-loop system and minimizes the $\mathcal{H}_2$ norm $\|T_{zw}\|_2$ of T_{zw}. Note that matrix $D(\boldsymbol{\xi}) = 0$ in order to guarantee that $\|T_{zw}\|_2$ is finite for every internally stabilizing and strictly proper controller. The technique used for controller design relies on results available in (Ghaoui and Niculescu, 1999) and (Scherer and Weiland, 2000), after being rewritten for the case of polytopic LPV systems. In the following, $\text{tr}(L)$ denote the trace of matrix L.

Result 6. A static state feedback controller guarantees the γ upper-bound for the continuous-time $\mathcal{H}_2$ norm of the closed loop operator $T_{zw}(\boldsymbol{\xi})$ with $\boldsymbol{\xi} \in \Xi$, that is,

$$\|T_{zw}(\boldsymbol{\xi})\|_2 < \alpha, \forall \boldsymbol{\xi} \in \Xi \tag{13}$$

if there are real matrices $X = X^T \succ 0$, $Y \succ 0$ and W such that

$$\begin{bmatrix} A(\boldsymbol{\xi})\,X + X\,A(\boldsymbol{\xi})^T + B(\boldsymbol{\xi})\,W + W^T\,B(\boldsymbol{\xi})^T & B_w(\boldsymbol{\xi}) \\ B_w(\boldsymbol{\xi})^T & -I \end{bmatrix} \prec 0$$

$$\begin{bmatrix} Y & C(\boldsymbol{\xi})\,X + E(\boldsymbol{\xi})\,W \\ X\,C(\boldsymbol{\xi})^T + W^T\,E(\boldsymbol{\xi})^T & X \end{bmatrix} \succ 0$$

$$\text{tr}\,(Y) < \gamma^2\,.$$

for all $\boldsymbol{\xi} \in \Xi_0$. The respective controller gain matrix is given by $K = W\,X^{-1}$.

The optimal solution for the continuous-time $\mathcal{H}_2$ control problem is approximated through the minimization of γ subject to the LMIs presented in Result 6.

6. IMPLEMENTATION AND RESULTS

To perform accurate structure inspection, an autonomous helicopter is required to cover the selected surfaces of the structure comprehensively in order to detect cracks, corrosion, etc. Recalling that the parameter vector is given by $\boldsymbol{\xi} = \begin{bmatrix} \rho_c & \alpha_c & \dot{\psi}_c & v_{z_c} \end{bmatrix}$, in the proposed case study the error space is partitioned into 945 overlapping convex regions, with 2^4 vertices each. The parameters are partitioned as follows: $\rho_c \in [4, 15]$ m into 3 intervals; $\alpha_c \in [-100, 100]^\circ$ into 9 intervals; $\dot{\psi}_c \in [-14, 14]^\circ/s$ into 7 intervals; and $v_{z_c} \in [-0.6, 0.6]$ m/s into 5 intervals. The state space matrices of the continuous-time systems (12) are approximated by affine functions of $\boldsymbol{\xi}$ using least squares fitting, yielding an average relative error on the matrices entries of less than 2.19 % in all the zones defined above.

6.1 Control Synthesis

The linear state feedback controllers were derived to meet the following design specifications: *i*) Achieve zero steady state error for the error variable $\mathbf{y}_e$ defined below and *ii*) Ensure that the actuators are not driven beyond their natural actuation bandwidth, that is $10\,rad/s$.

The integral of $\mathbf{y}_e = \begin{bmatrix} \boldsymbol{\eta}_e^T & \psi_e \end{bmatrix}^T$ is included in the design as a performance output to guarantee that the closed loop system has zero steady-state error in response to laser-based position and yaw angle commands. To meet the specified design requirements, additional dynamics weights on the disturbances and inputs, as well as simple weights on state and performance output, were introduced using the same approach as in Guerreiro et al. (2007).

The controller implementation scheme is based on the D-methodology comprehensively described in (Kaminer et al., 1995), which provides auto-trimming and straightforward implementation of anti-windup schemes due to the placement of the integrators at the plant's input.

6.2 Simulation Results

The simulation results herein presented were obtained using the nonlinear dynamic model SimModHeli, parameterized for the Vario X-Treme model-scale helicopter. The specific application addressed in this paper (automated inspection of concrete bridge piers) motivated the design of a simulation setup that can effectively be used to evaluate the performance of the overall closed loop system in a real mission scenario. For that purpose the vehicle is required to track the trajectory shown in Figure 1 and composed by: *(i)* an ascending helix keeping the vehicle facing the pier ($\rho_c = 10$ m, $\alpha_c = 0^\circ$, $\dot{\psi}_c = 0.2^\circ/s$ and $v_{z_c} = -0.4$ m/s); and *(ii)* stationary hover at a close location relative to the pier ($\rho_c = 9$ m, $\alpha_c = \dot{\psi}_c = v_{z_c} = 0$). In addition to noise generated using the Von Karman disturbance model (with variance [0.98 0.98 0.5] $m^2\,s^{-2}$, respectively in the x, y and z components of the wind velocity), a discrete wind gust with amplitude 2.5 m/s and rising time of 10 s is applied at time $t = 20$ s to all velocity components.

The laser kinematics errors described by the helicopter and corresponding actuation errors are represented in Figure 3, where the blue dashed lines and the red solid lines represent, respectively, the simulation with and without wind disturbances. As shown in the figure, the transitions between the ascending helix and hover display a smooth behavior and the trajectory tracking errors without wind disturbances are very small. It can be also concluded that the controller is able to reject the wind disturbances, reacting to the changes in directions along the helix,

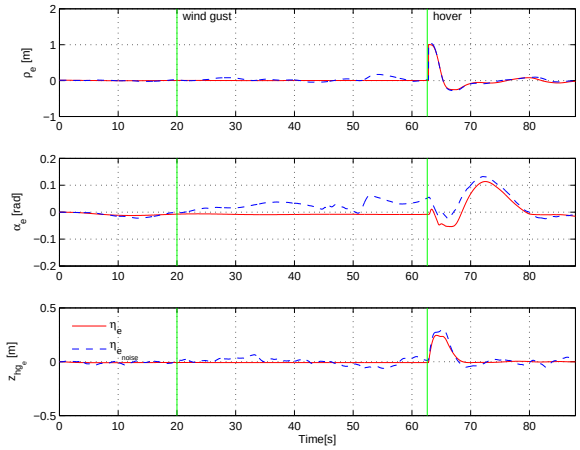

(a) Laser kinematics error $\boldsymbol{\eta}_e$

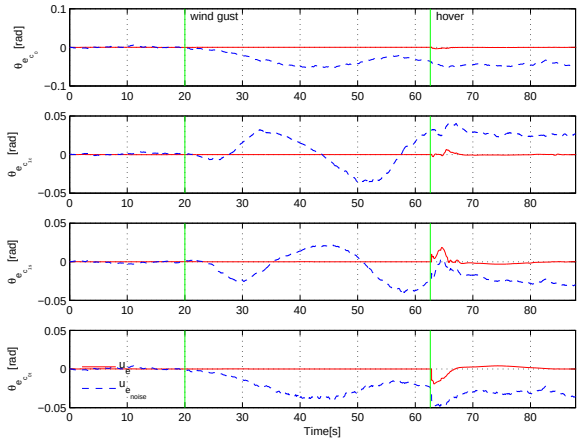

(b) Actuation error $\mathbf{u}_e$

Fig. 3. 3-D laser-based trajectory following results (red solid line – without wind disturbance; blue dashed line – with wind disturbances.

and the overall vehicle trajectory only deviates from the reference when discrete wind gusts are applied and in the abrupt transition from the helix to hover. Nonetheless, excluding the hover transitory, the maximum tracking errors in the presence of wind disturbances do not exceed 18 cm for ρ, 3.6° in α and 7 cm in z_{hg}.

7. CONCLUSIONS

This paper presented the design and performance evaluation of a 3-D trajectory tracking laser-based controller for autonomous helicopters, motivated by the automatic inspection of large infrastructures were GPS signal is not reliable. The major contribution of this work is the introduction of a laser nonlinear kinematics, formulated in 3-dimensions, and a trajectory-dependent error space defined to express the dynamic model of the vehicle and the laser kinematics. Resorting to an $\mathcal{H}_2$ controller design methodology for affine parameter-dependent systems, the presented technique exploited an error vector that naturally describes the particular dynamic characteristics of the helicopter for a suitable flight envelope. For a given set of operating regions, a nonlinear controller was synthesized and implemented under the scope of gain-scheduling control theory, using a piecewise affine parameter-dependent model representation. The effectiveness of the proposed control laws was assessed in the MATLAB/Simulink simulation environment with a nonlinear model of the helicopter in a realistic mission scenario. The quality of the results obtained clearly indicate that the methodology presented is well suited to be used in the proposed application.

REFERENCES

Craig, J. (1986). *Introduction to Robotics: Mechanics and Control*. Addison-Wesley Publishing Company, Massachusetts, 2nd edition edition.

Cunha, R. (2002). *Modeling and Control of an Autonomous Robotic Helicopter*. Master's thesis, Department of Electrical and Computer Engineering, Instituto Superior Técnico, Lisbon, Portugal.

Cunha, R., Antunes, D., Gomes, P., and Silvestre, C. (2006). A path-following preview controller for autonomous air vehicles. In *AIAA Guidance, Navigation and Control Conference*. AIAA, Keystone, CO.

Cunha, R., Guerreiro, B., and Silvestre, C. (2005). Varioxtreme helicopter nonlinear model: Complete and simplified expressions. Technical report, Instituto Superior Técnico, Institute for Systems and Robotics.

Ghaoui, L. and Niculescu, S.I. (1999). *Advances in Linear Matrix Inequality Methods in Control*. Society for Industrial and Applied Mathematics, SIAM, Philadelphia, PA.

Guerreiro, B., Cunha, R., Silvestre, C., and Antunes, D. (2007). Trajectory tracking h2 controller for autonomous helicopters: and aplication to industrial chimney inspection. In *17th IFAC Symposium on Automatic Control in Aerospace*. Toulouse, France.

He, R., Prentice, S., and Roy, N. (2008). Planning in information space for a quadrotor helicopter in a gps-denied environment. In *IEEE International Conference on Robotics and Automation*, 1814–1820. Pasadena, CA, USA.

Kaminer, I., Pascoal, A., Khargonekar, P.P., and Coleman, E.E. (1995). A velocity algorithm for the implementation of gain-scheduled controllers. *Automatica*, 31(8), 1185–1191.

Leonard, J.J. and Durrant-Whyte, H.F. (1991). Mobile robot localization by tracking geometric beacons. *IEEE Transactions on Robotics And Automation*, 7(3), 376–382.

Padfield, G.D. (1996). *Helicopter Flight Dynamics: The Theory and Application of Flying Qualities and Simulation Modeling*. AIAA Education Series. AIAA, Washington DC.

Parke, G. and Hewson, N. (eds.) (2008). *ICE Manual of Bridge Engineering*. Institution of Civil Engineers, London, UK, second edition.

Scherer, C. and Weiland, S. (2000). Lecture notes on linear matrix inequality methods in control. Dutch Institute of Systems and Control.

Silvestre, C. (2000). *Multi-objective Optimization Theory with Applications to the Integrated Design of Controllers/Plants for Autonomous Vehicles*. Ph.D. thesis, Instituto Superior Técnico, Universidade Técnica de Lisboa, Lisbon, Portugal.

Thrun, S., Fox, D., Burgard, W., and Dellaert, F. (2001). Robust monte carlo localization for mobile robots. *Artificial Intelligence*, 128(1-2), 99–141.